Additive Manufactured ULTEM 9085 Part Qualification and Allowable Generation

Reza Hajiha[1], Harsh Baid[1], Steven Floyd[2], Nicole Curtis-Brown[2], Nima Moazami[1], Frank Abdi[1,] and Elizabeth Clarkson[3]

[1]*AlphaSTAR Corporation, Long Beach, CA, USA*
[2]*Northrop Grumman Space Systems-Space Park, CA, USA*
[3]*National Institute for Aviation Research, Wichita State University, Wichita, KS, USA*

ABSTRACT

Part qualification of additive manufactured polymers has become more important due to the increasing tendency in industrial application of Fused Deposition Modeling (**FDM**) which yields to quality parts with low cost of manufacturing and high freedom of customization. To reduce printing errors and evaluate fabrication process designs before actual manufacturing, reliable virtual methods are required to model the material, predict part performance, determine the design allowables regarding the variations in material, printing errors and manufacturing facilities.

This case study demonstrates thermo-mechanical analysis, print process simulation, allowable generation and validation of FDM based 3D printed **ULTEM 9085** material system. A nano assisted micromechanics approach is implemented to predict room temperature mechanical properties of 3D printed material system considering micro voids as inclusion calculated using thermal transport phenomenon. The case study also includes prediction of temperature dependent mechanical properties of FDM printed unfilled ULTEM 9085 material using multi-scale material modeling, cure kinetics and multi-factor technique. From print process modeling point of view, geometrical and pathing error macro size defects, called "bald spot", were calculated and resulted in degradation of both modulus and strength properties in the element scale of the Finite Element Model (FEM). Next, thermal and coupled thermal structural analysis using Multi-scale Progressive Failure Analysis (MS-PFA) were performed to calculate temperature distribution, deformation and residual stress during and after 3D printing process. Finite Element Analysis of service loading integrated with MS-PFA was also performed on virtually 3D printed parts considering residual stress and deformed shape as well as geometrical and pathing errors. The simulation showed excellent agreement with available test data. Also, damage initiation and evolution were predicted as a result of MS-PFA. By performing virtual sampling, the tensile strength allowables and constituents' sensitivities for ULTEM9085 printed in multiple orientations were predicted and validated with NIAR's qualification and Stratasys's equivalency test data. The generic acceptance region for parts printed by RP+M and Stratasys printers were plotted to establish FDM ULTEM9085 generic acceptance region between those two distinguished manufacturing facilities.

Keywords: **1**) Fused Deposition Modeling; **2**) ULTEM 9085; **3**) Micro Void; **4**) Nano assisted Micro Mechanics; **5**) Temperature Dependent Mechanical Properties; **6**) Geometrical and Pathing Errors; **7**) Coupled Thermal-Structural Analysis; **8**) A-B and Generic Basis Allowables

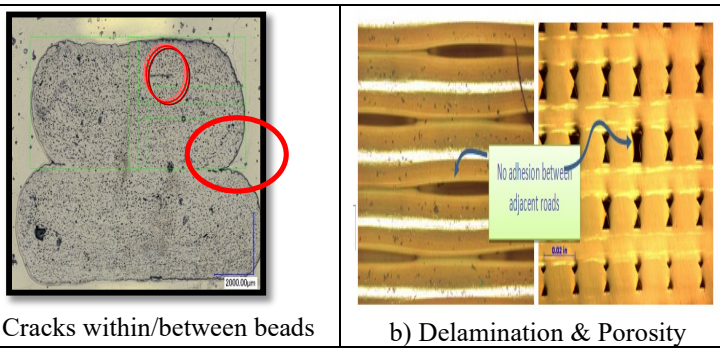
Copyright 2020. Used by the Society of the Advancement of Material and Process Engineering with permission.

NOMENCLATURE

Notation	Description
CDF:	Cumulative Distribution Function
***CTE*:**	Coefficient of Thermal Expansion
***D&DT*:**	Durability and Damage Tolerance
ET:	Elevated Temperature
***FDM*:**	Fused deposition Model
***FFF*:**	Fused Filament Fabrication
ICME:	Integrated Computational Material Engineering
MCQ:	Multi-scale material characterization and Qualification
***MS-PFA*:**	Multi Scale Progressive Failure Analysis
***RT*:**	Room Temperature
***TG*:**	Transient Glass Temperature
***TMg*:**	GENOA 3DP Thermal Management
***VVR*:**	Void Volume Ration

1. INTRODUCTION

Additive Manufacturing (AM) continues to show great promise. AM technology has demonstrated an ability to decrease costs and reduce manufacturing lead-time, while providing capability to fabricate complex geometries that are otherwise impossible using conventional manufacturing processes. *Yet challenges* remain with AM that makes part qualification difficult. Builds are reliant upon experimentally driven trial and error, and NDE (nondestructive evaluation) data driven analysis is not properly exploited to detect and possibly correct build anomalies. Common problems associated with **Polymers**, with and without inclusions, build problems include *porosity (gas bubbles, inter-bead voids, fiber pull out), interlayer delamination, wrinkling, warpage, anisotropic behavior, residual stress, fiber waviness/agglomeration and saturation of mechanical (strength/stiffness) properties* (**Figure 1**). The manufacturing anomalies, in terms of effects of defects, are the source of scatter and uncertainty in mechanical and fatigue properties for both metal and polymer AM parts. In general AM process often produces part with unique microstructural irregularities in metals, plastics, and fibrous composite material. **Figure 7** shows typical inter-bead void formation for two different 3D printed meso-structures. **Table 1** describes the **FDM** machine parameters



a) Cracks within/between beads b) Delamination & Porosity

Figure 1. Micrographs of polymer meso-structures, showing typical defect formation

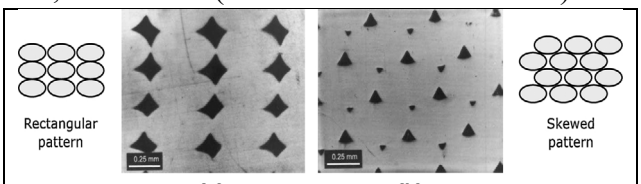


Figure 2. Micrographs and schematics of two different meso-structures, a) rectangular and b) skewed, showing typical triangular void formation [11]

PROBLEM: The AM process that is being considered in this paper is FDM. Typical FDM exhibits high porosity, sub-optimal bonding between roads and layers, poor interfacial bonding between polymer and fillers. Proper material modeling is needed to assist in process optimization and printed structure performance modeling. It is also observed that during the print process temperature gradient between two layers leads to: **1)** contraction of hot layer and compression of cold layer until equilibrium is achieved; and **2)** thermal stresses generated during solidification process induces thermal warping/distortion in 3D printed part.

Table 1. Thermoplastic AM machines primary printing parameters.

Items	Parameters	Description	Controlled or Predefined
1	Printing Speed	Velocity of nozzle across surface	Controlled
2	Print Pattern	Island, Ox, Concentric, rectangular	Controlled
3	Hatch Spacing	Distance between neighboring passes	Controlled
4	Layered Thickness	Hight of single layer	Controlled
5	Nozzle Temperature	Polymer Extrusion Temperature	Controlled
6	Nozzle Diameter	Extrusion dimension	Controlled
7	Extrusion Speed	Polymer feeding Velocity	Controlled
8	Baseplate temperature	Build plate temperature	Controlled
9	Baseplate Type	Material of Base plate	Controlled
10	Chamber Temperature	Enclosed Space Temperature	Controlled
11	Inclusion Volume Ratio	Material, and type	Controlled
12	Beed Width dimensions	Based on Hatch Spacing, Print speed, Nozzle diameter	Uncontrolled

The mechanical behavior of **FDM** specimen including the effect of build parameters is being extensively studied to understand the variation in mechanical and thermal properties [2-**4**]. Researchers have studied the effect of layer thickness, deposition angle as well as infill on the flexural properties [2]. Studies have been also conducted to see the compressive properties variation due to raster angle, air gap and wall thickness **[3].** Finite Element Analysis has also been studied in great extent by many researchers to perform additive manufacturing process [4-**5**]. Finite element method has been implemented by researchers [4] to evaluate the temperature distribution during the **FDM** simulation process. Others have developed FE methods [5] to calculate mechanical properties of **FDM** parts validated with test.

One of the primarily focus of this paper is simulation of 3D printing process using ULTEM 9085 material. For appropriate simulation of 3D printing process, it is very important to assign temperature dependent material properties (both thermal and mechanical). The temperature dependent mechanical properties are either obtained from test or assumed based on some degradation factor. The 3D printing simulation can lead to totally different directions depending on the assumed thermal dependent mechanical properties. The thermal stress calculated from 3D printing simulation process could be totally different depending on the assigned thermal dependent mechanical properties. The prediction of the structural performance due to service loading could be totally different depending of the residual stresses generated during the 3D printing simulation process. If the temperature dependent material property is not known, an appropriate methodology/technique is needed to be implemented to predict accurate properties. This paper also focuses on cure kinetics-based method coupled with multi-factor technique to predict temperature dependent material properties (stiffness and strength). The predicted temperature dependent material properties are implemented in FE model generated using 3D printing process to perform coupled structural and thermal analysis. A three-point bending simulation is carried out and the flexural stress-strain curve is validated with test available in the literature for **ULTEM 9085** material [6].

This paper describes the effort of **FDM printed** ***Neat (Unfilled) Ultem 9085 thermoplastic material, ASTM coupons, and sub-component utilizing ICME tool set for multi-scale material modeling, and process modeling.*** **Material modeling** included prediction of: 1) Thermal state and Material State using Micro thermal Management (**GENOA 3DP TMg**) thermal transport software, **2)** Multi-scale material characterization and Qualification (**MCQ**) modeling including prediction of: (i) mechanical properties (modulus, strength) Vs. Temperature, and **b)** Material qualification, and generation of probabilistic A_ B basis allowables and perform generic equivalency using different machines. **Process Modeling** included: **a)** detection of macro voids and defects due to print pattern error, prediction of loss of stiffness and strength and **b)** formation of residual stress, of dog bone, and cross beam box distortion during AM printing process considering effect of defects.

Machine Equivalency: Generic Basis Equivalency are determined in NIAR report [8-9] using Rapid prototyping and Manufacturing (RP+M) facilities as a part of material qualification. Stratasys AM machine then, performed some tests using its own manufacturing facilities as a part of equivalency process. This effort shows the validation of A & B Basis allowables for NIAR [9] Qualification report. Then, by performing virtual sampling, the allowables for parts printed by Stratasys facilities are predicted .Consequently, the generated virtual samples are used to define the Generic basis values and plot the Generic acceptance region for ULTEM 9085 FDM printed material system between two distinguished Additive manufacturing machines.

2. METHODOLOGY

The entire 3D printing process for XY direction (**Figure 2**) was carried out in three key steps: (**1**) Micro-Thermal Modeling (**2**) material modeling, and (**3**) 3D printing process modeling. The flow process of the material model, and printing process is shown in **Figure 3**. First, the air bubbles content appearing during the FDM printing was predicted using GENOA 3DP TMg (1 % air bubbles). Material modeling is required to assist in process optimization and printed structure performance modeling. Material modeling is conducted using nano-micro mechanics algorithm to predict the desired room temperature and elevated temperature (RT/ET) mechanical material properties (strength, stiffness) of ULTEM 9085 resin. Cure Kinetics was coupled with multi-factor technique to predict temperature dependent stiffness and strength of unfilled ULTEM 9085 material. From process modeling point of view, 3D printing simulation using the developed process parameter for FDM fabrication such as print pattern is performed to calculate the residual stress, and distortion of heat affected zone.

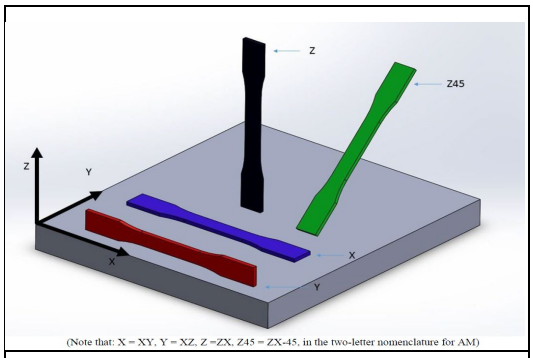


Figure 2. Demonstration of printing orientations including XY

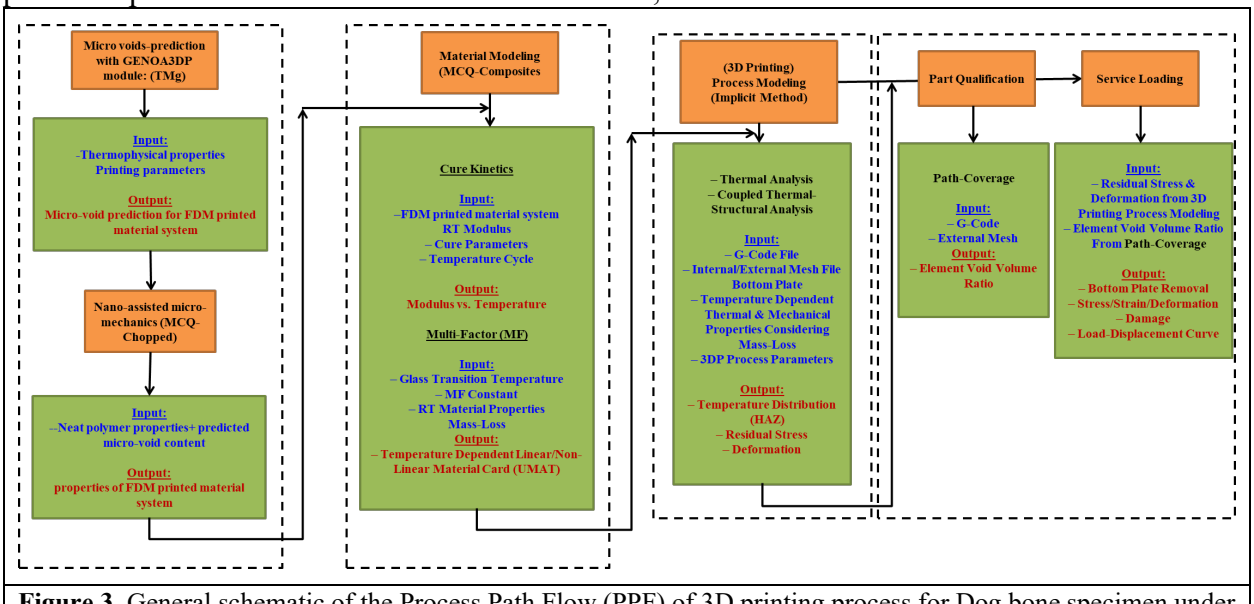


Figure 3. General schematic of the Process Path Flow (PPF) of 3D printing process for Dog bone specimen under tension loading using 3D printed ULTEM9085.

2.1 GENOA 3DP PathCoverage -Print Error Detection: *Macro Void Detection Software*

Before significant resources are committed to print a part, it is a good idea to assess the coverage of the printer paths on the printed part. This tool, GENOA 3DP PathCoverage, supports **a**) Quick visual assessment of printer GENOA 3DP PathCoverage, and **b**) Void ratio computation for all elements. This 2D graphics code displays one printed layer at a time. It supports quick switch (single key press) to the next or previous layer. The width and semi-circular end caps of each path are shown accurately on the part, given a user- specified bead width for the paths. Hence, a quick look can often reveal problems in GENOA 3DP PathCoverage. Further, a user can zoom in up close to verify minor coverage "leak". There is a mode to facilitate the identification of problematic paths. For better visualization of void detection, a part fabricated using Fused

Deposition Modeling (**FDM**) is compared with GENOA 3DP PathCoverage results in **Figure 4.** If the part is already printed by a defective set of paths, a user can choose to have the void ratio for each element

of a FEM computed by this code, so that further quality assessment can be performed by a simulation code that accounts for such coverage voids.

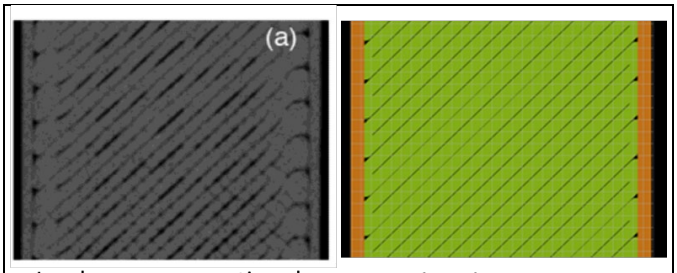


Figure 4. GENOA 3DP PathCoverage Bald Spot detection [1]

2.2 Material Modeling Thermo-Mechanical)

2.2.1 Micro Thermal Management (GENOA 3DP TMg)

A novel algorithm called Zeroth Order-Model (ZOM) and advanced Thermal code was developed based on systematic semi-analytical and Finite-Difference Explicit Method (FDEM)) approach. This multi-physics multi-phase (powder, solid, and liquid) model predicts real-time calculation of through-the-thickness temperature versus time and location in a more efficient way compare to other FEM. It has an advantage of extremely fast calculation and high accuracy (both macro- and microscale level). The algorithm is applicable to different class of materials such as metal-powder, Neat and reinforced polymer, and ceramic which proposes. Approach that addresses all thermal states/regions including i) heating, **ii**) melting, **iii**) melt-superheated **iv**) superheat-cooling v) solidification/sintering as well as **vi**) cooling depending on AM process condition and definition. The transient temperature gradients are calculated to predict the heat conduction, convection, radiation, axial and radial laser irradiation and absorption based on Gaussian distribution in laser-based concepts or a heat flux to the liquefier during **FFF** and **FDM** AM processes. This multi-physics multi-phase (solid, powder and liquid) module aims to compensate for the systematic physical property variabilities of the powder bed layer (e.g. density and volume changes, Volume of Solid (**VOS**), void formation, shrinkage, liquid formation and movement due to melting) and to determine process parameters for the subsequent layers to correct the defects in previous layers. This tool would be able to control the depth/width of the melt pool and Heat Affected Zone (**HAZ**) to deliver more energy to partially melted regions or less energy to overheated regions. **Figure 5** shows an example of FDM 3D Print Temp. Map. Equation 1 represents the main heat transfer equation that has been used in temperature calculation. In this equation, , $\boldsymbol{\rho}$ stands for density, $\boldsymbol{l}$ stands for material-phase, $\boldsymbol{C_p}$ is specific heat capacity, $\boldsymbol{V}$ is the volume of the element, $\boldsymbol{Q_s}$ is the heat source (laser or nozzle liquefier), $\boldsymbol{Q_k}$ is thermal conductivity, $\boldsymbol{Q_r}$ is thermal radiation, $\boldsymbol{Q_c}$ is thermal convection, and $\boldsymbol{i, j, k, t}$ stand for 3 different special directions and time step.

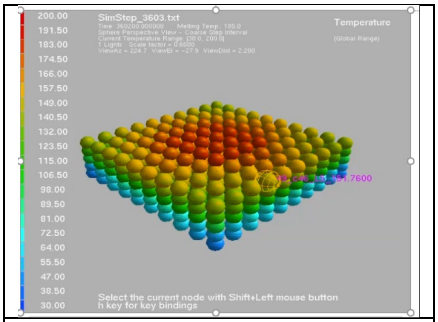


Figure 5. FDM 3D Print Temp. Map

$$\rho_l C_{pl} V \frac{dT(i,j,k)}{dt} = Q_s(i,j,k,t) - Q_k(i,j,k,t) - Q_r(i,j,k,t) - Q_c(i,j,k,t) \qquad [1]$$

2.2.2 Material Characterization and Qualification (MCQ):

The micromechanical composite models account for damages and defects that are typical of composites for as many extreme conditions as the parts will experience. MCQ's micromechanical material modules can compute responses of lamina and laminate levels and produce mathematical

representations of the composite during any state of load progression (stress, strain, damage, no damage, etc.) and give those representations to a finite elements solver to run the necessary the analysis. It generates thermal, structural, electrical, and hygral properties and degradation under service environments for progressive failure analysis. Responses at each scale are automatically used as the loads to smaller scales (layer stresses are used to determine fiber/inclusion/matrix/interphase stresses – some micromechanics simulations or some layers will not use fibers). The composite damaged state stiffness and strength recomputed and are fed back into the FE model for the next load step (**Figure 6**). Material Characterization and Qualification (MCQNANO) includes **a**) Calibrate material properties using MCQNANO; and **b**) Predict the strength for each bead using the MCQNANO.

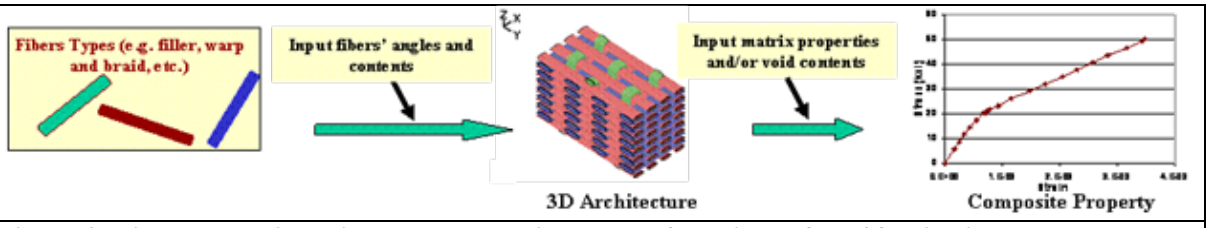


Figure 6. Micro-mechanics unit cell model considers manufacturing defects / fabrication parameters

2.2.3 Nano-Micro Mechanics based Material Property Prediction:

Many micromechanics approaches have been developed for the evaluation of the overall properties of heterogeneous materials and their dependence on the properties of constituents and the microstructure of materials. They are mainly based on Eshelby equivalent inclusion theory. A nano-micro mechanics-based material modeling approach is implemented to predict short fiber reinforced ABS material system Room Temperature (RT) mechanical properties including air particles as void and weak fiber matrix interface. The proposed multi-scale material modeling methodology combines Mori-Tanaka effective far-field theory **[7]** and micro-mechanics [10] to predict the desired material properties of 3D printed filled ABS material system.

In the suggested approach, the effective nanocomposite (or enhanced matrix) material properties, where carbon nanotubes of known weight fraction are aligned in a neat matrix, are determined first analytically. The analysis approach uses well-known Mori-Tanaka formulation [7] for calculating the anisotropic nanocomposite properties from isotropic matrix and nano-particles properties (stiffness, aspect ratio and volume fraction). In an independent review, Tucker and Liang (1999) found that Mori-Tanaka type models give the best results for large-aspect-ratio fillers (nanoparticles). For a composite material reinforced with aligned fiber-like particles, the Tandon and Weng (1984) prediction of the moduli E_{11} (aligned particle direction), E_{22} (transverse to the aligned particle direction), the in-plane shear modulus G_{12}, and the out-of-plane shear modulus G_{23} of the composite are:

$$E_{11} = E_m \Big/ \left(1 + f_p\left(A1 + 2\upsilon_m A2\right)/A\right) \tag{2}$$

$$E_{22} = E_m \Big/ \left(1 + f_p\left(-2\upsilon_m A3 + \left(1-\upsilon_m\right)A4 + \left(1+\upsilon_m\right)A5 * A\right)/\left(2A\right)\right) \tag{3}$$

$$G_{12} = G_m \Big/ \left(1 + f_p\left(\mu_m/\left(\mu_p - \mu_m\right)\right) + 2\left(1-f_p\right)H_{1212}\right) \tag{4}$$

$$G_{12} = G_m \Big/ \left(1 + f_p\left(\mu_m/\left(\mu_p - \mu_m\right)\right) + 2\left(1-f_p\right)H_{2323}\right) \tag{5}$$

where A and A_i are constants depending on the components of the Eshelby tensor and the matrix/nano-particles properties, and H_{ijkl} are the Cartesian components of the Eshelby tensor.

2.2.4 Multi-Factor Technique Based Temperature Dependent Material Strength Properties Prediction

Mechanical properties (Tensile and Compressive Strength) are calculated as a function of temperature using multi-factor technique along with progressive failure analysis. The strength properties are calculated using Equation-6, a multi-factor technique as a function of glass transition temperature. In Equation-6 $\boldsymbol{\sigma_o}$ is room temperature strength property, $\mathbf{T_g}$ is the glass transition temperature, $\mathbf{T_o}$ is the temperature of interest and α is the multi-factor coefficient.

$$\sigma = \sigma_o \left[(T_g - T)/(T_g - T_o)\right]^{\alpha} \quad (6)$$

2.2.5 Cure Kinetics Based Temperature Dependent Material Properties Prediction

Mechanical property (Modulus) is calculated as function of temperature. The approach utilizes a micro-mechanics fiber/matrix-based progressive consolidation process. The constituent stiffness is updated based on degree of cure predicted by cure kinetics. The proposed simulation process will account for the transient heat transfer and temperature distribution through parts by time-history incremental simulation of the curing process. Viscosity of the resin is determined as a function of the degree of cure simulated by the Bogetti/Gillespie [12] model.

2.3 3D Printing Process Modeling; Thermal and Coupled Thermal-Structural Analysis

3D printing process modeling is categorized into two steps i.e. **thermal** and **coupled thermal-structural** analysis. 3D numerical model was developed to perform thermal and coupled thermal-structural analysis for XY build direction dog bone specimen with 0°/90° orientation. G-Code file was generated using Slic3r software for XY build direction. The G-Code file was used to specify the actual paths performed during the printing process. Finally, a detailed re-construction of the model was generated for FE analysis.

The coupling between the thermal and mechanical field can be obtained by a sequential solution procedure. The sequentially coupled thermal-structural analysis is used when the structural responses depend on the temperature field, but the temperature field can be found without the effect of stress/deformation field. This means that the heat transfer analysis is first performed to determine the temperature field. The temperature field is calculated considering conduction, boundary convection, and boundary radiation. Heat transfer numerical analysis is implemented to model solid body heat conduction with temperature dependent conductivity and specific heat, general convection, and radiation boundary conditions. The heat transfer analysis is nonlinear due to: **a**) temperature dependent material properties, **b**) nonlinear boundary conditions (film coefficient can be function of surface temperature). Then, the calculated temperature field is used as an input to the coupled analysis. Since the material is temperature dependent, the material properties change as a function of the temperature field during the fabrication simulation. For heat transfer analysis, FDM process modeling was used by assigning constant thermal boundary values to the added elements.

2.4 Test Reduction by Composite Strength Allowables Determination

A- and B-basis strength values determination for materials are vital to achieve the structural design with acceptable safety and confidence level in order to reduce the risk in aerospace industry. The possibility of failure is lowered for significant aircraft structures by considering A and B-basis design values throughout the whole design process. While the 3D printed parts properties show scatter due to constituents, environmental conditions and architectural variations some criteria are required to determine the Printed material tolerance with certain levels of confidence. For A-basis,

at least 99% of the material strength values population are anticipated to be equal or exceed this tolerance magnitude with a confidence level of 95%. B-basis values are applied to structures and components considered as redundant and less critical where failure results in safe load redistribution. For B-basis, 90% of the material strength population values are expected to be equal or exceed B-basis strength value with 95% of confidence level. The method to define strength allowables with test reduction is based on existing accepted standards and practices [8, 9]. It uses statistics from lamina level testing to reverse engineer uncertainties in composite constituents' properties variations and deviations derived from fabrication process (**Figure 7**).
Afterwards, the uncertainties are implemented in CLM-RM to generate random virtual test samples for un-notched specimens used instead of actual test samples. The methodology combines probabilistic methods with progressive failure analysis (PFA) and Bayesian statistics to reduce the number of tests needed to define of A- and B-basis strength values. [14]. There are three discrete proficiencies (options) to generate the A and B basis Allowables:

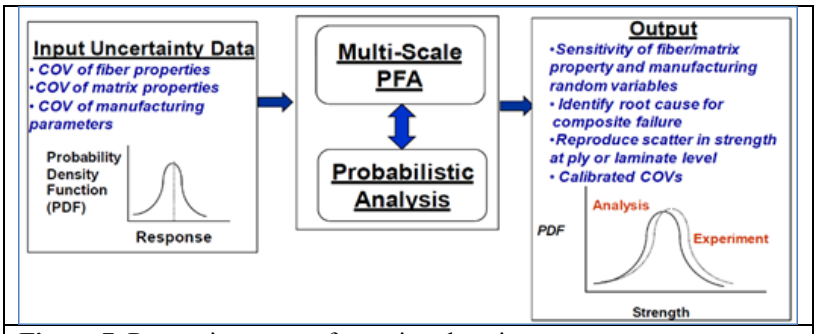


Figure 7. Recreating scatter from virtual testing process

1. **Test data procured by the user** – Method is a combination of deterministic and statistical approach elaborated in CMH-17(Composite materials handbook) and FAA CFR 14 (Aeronautics and space).

2. **Reduced test data** (1 coupon from each batch) –A combination of progressive failure analysis with probabilistic methods. Generic basis allowable is used to improve upon CVM allowable generation.

3. **Lack of test data** – This method is a combination of probabilistic approaches, based on standard practices, and progressive failure analysis. The calculation is based on the scatter recreation in lamina strength caused by variations in fiber/matrix properties and fabrication defects within an appropriate margin error (~±10%). The approach has been validated by comparing its A/B-basis predictions with values obtained from standard methods using test data from robust or reduced sampling. **Figure 8** shows technical sequences to define A- & B- basis allowables. The results of PFA analysis on unnotched virtual samples were the input to CMH-17 methodology for A-B Basis determination. The virtual random sampling generates a full Cumulative Distribution Function of Response (CDF) for the composite laminate strength. The A/B-basis values are then easily extracted from the CDF curve at 0.01 and 0.1 probabilities, respectively. [14].

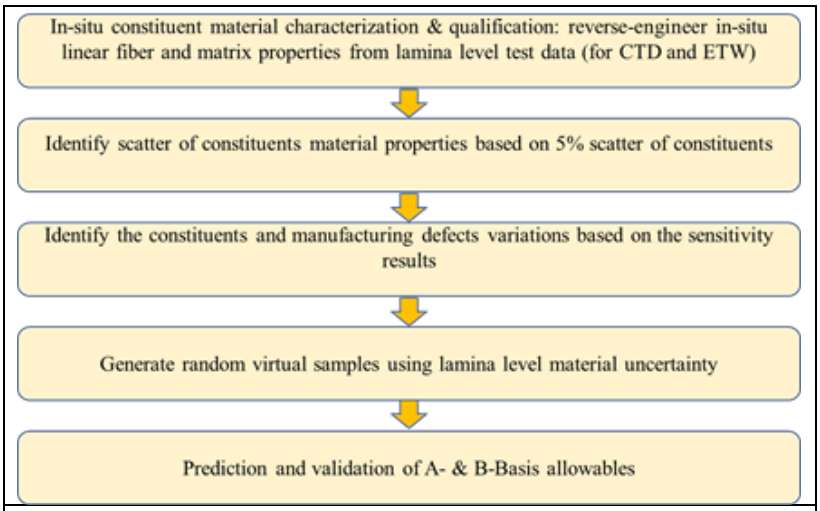


Figure 8. Technical sequences to determine A- & B-basis [14]

2.5 Computing the Generic Acceptance Region

The multivariate 95% confidence ellipsoid represents the generic acceptance region based on the NCAMP dataset. The boundary of the generic acceptance region for strength equivalence is defined to be lower edge of the multivariate 90% certainty ellipsoid for a single unit mean vector established on the NCAMP dataset. These regions are determined through the computation of the population covariance matrix, Σ, the population mean vector. The equation for the generic acceptance region **[14]**:

$$N(v - M_1)'\Sigma^{-1}(v - M_1) \leq c \quad (7)$$

Where,

- N = 1 because this is the region for a single unit
- v is any p-dimensional vector such that the equation is true (p is the number of different tests in a complete unit).
- M_1 is the p-dimensional mean vector computed from all units in the NCAMP database.
- Σ is the p×p covariance matrix computed from all complete units in the NCAMP database
- c is the appropriate percentile of a distribution

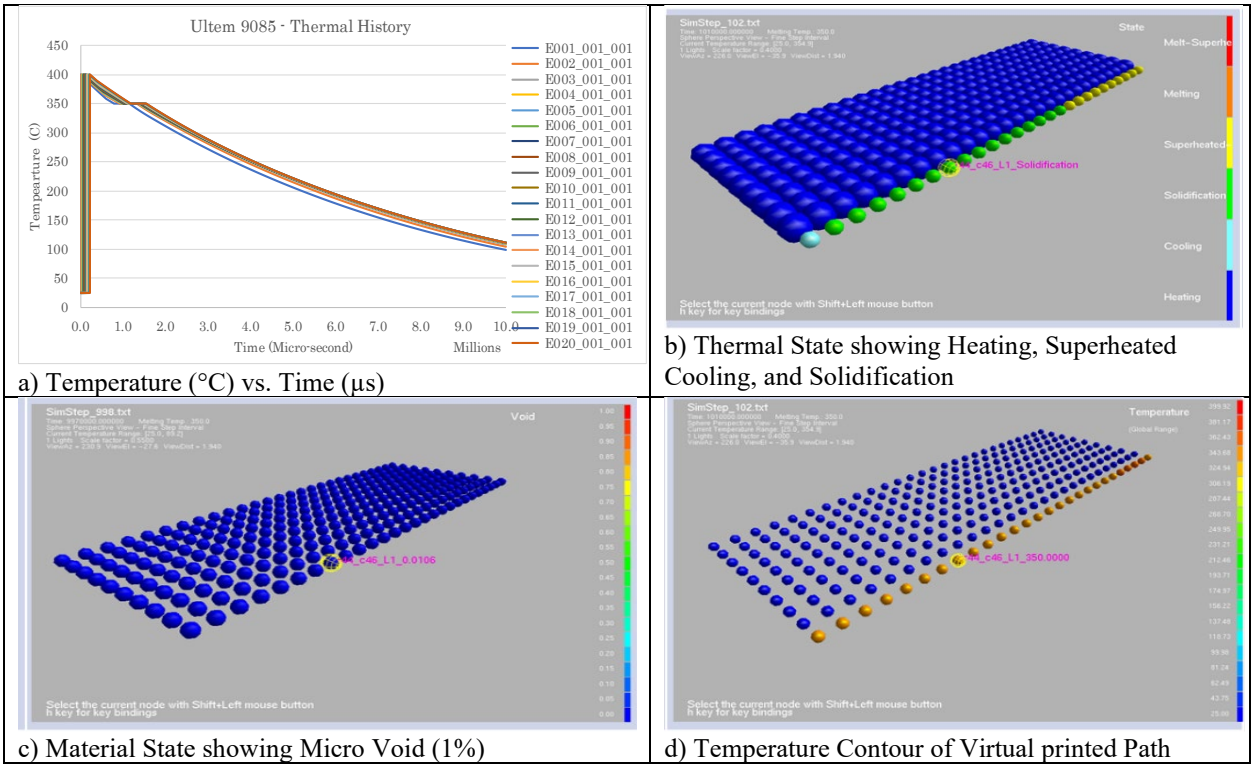
The acceptance and equivalency regions are ellipses when only two properties are in a group. The concept is extended to a multi-dimensional ellipsoid for more than two properties. This multidimensional ellipsoid is projected to a 2-dimensional ellipse for the graphical representation of those properties **[14]**.

3. RESULTS AND DISCUSSION

The entire 3D printing process was carried out in three key steps: **Material Modeling** including the prediction and implementing the micro void content to determine printed ULTEM 9085 properties as well as prediction and validation of elevated temperature properties, **Process Modeling** of Fused Deposition and implementation of print errors known as Macro voids, and **Service Loading** performance.

3.1. Micro Thermal Modeling

Thermal History (**Figure 9a-b**) predicted including heating, melting, melt-superheating, superheat-cooling, solidification/sintering, and cooling periods. It also predicted **Material State** (i.e. transient density, volume of solid (VOS), and void volume ratios), **Figure 9c-d**. The model can be extended to account for multi-part interaction due to thermal gradient, and residual stress and the effect of print build orientation.



a) Temperature (°C) vs. Time (µs)

b) Thermal State showing Heating, Superheated Cooling, and Solidification

c) Material State showing Micro Void (1%)

d) Temperature Contour of Virtual printed Path

Figure 9. GENOA 3DP TMg: FDM Process, Thermal, Material State of ULTM9085

3.2 Micro-Mechanical Material Property Prediction Modeling at RT and ET):

The material modeling process includes calibration and validation of Room temperature printed ULTEM 9085 including the effect of micro voids predicted by **Micro Thermal Model** (1%). Further, it includes using neat material elevated temperature modulus to validate ULTEM 9085 Cure kinetics and predict the elevated temperature mechanical properties for the FDM extruded material which eventually contributed to generation of temperature dependent material card for the FEM solver.

3.2.1 Material Property Prediction at RT

A nano-micro mechanics-based material modeling approach is used to predict FDM extruded ULTEM 9085 Room Temperature (RT) mechanical properties including spherical air particles implementation as micro voids. The proposed multi-scale material modeling methodology combines Mori-Tanaka effective far-field theory **[7]** and micro-mechanics **[10]** to predict the desired material properties of extruded ULTEM 9085 resin. **Input:** The neat resin properties are obtained from San Diego Plastics Inc spec sheet **[15-16]**. **Assumption:** 1% of spherical air

particles with 20 µm diameter is assumed and is uniformly distributed in the resin; Stress-based failure criteria is implemented.

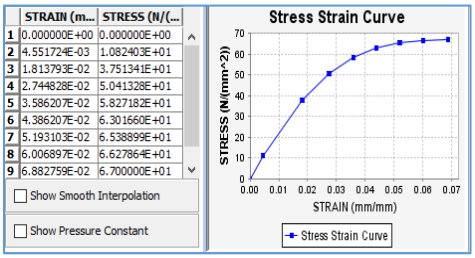
Output: The code outputs aligned 2D random, and 3D random room temperature material properties. The inputs, assumptions and outputs for material modeling (RT) is shown in **Figure 10a-e**. For the simplicity of this material modeling process only 3D random properties are considered. **Figure 10f** shows the Predicted Mechanical Properties (modulus, and strength of ULTEM 9085 at RT)

a) ***Input:*** *Air bubble particles (1%) from GENOA 3DP TMg*

Property	Magnitude
Density (tonne/mm^3)	1.205 E-12
Elastic Modulus (MPa)	0.1
Tensile Strength (MPa)	6.89 E-3
Compressive Strength (MPa)	6.89 E-3
Interface Shear Strength (MPa)	1.13 E2
Adhesion Factor	0.05

b) ***Input:*** *Neat Unfilled ULTEM 9085 Properties*

Property	Magnitude
Density (tonne/mm^3)	1.34
Elastic Modulus (GPa)	2.7
Poisson's ratio	0.4
Tensile Strength (MPa)	118.80
Compressive Strength (MPa)	151.68
Shear Strength (MPa)	113.42



c) ***Input:*** *Nonlinearity of ULTEM 9085 with pressure constant of 2 [15, 16]*

d) ***Assumption:*** *Air bubbles geometry and content (1% micro void content predicted by GENOA 3DP TMg)*

Property	Value
Shape	Spherical
Weight Ratio	9.08 E-6
Volume Ratio	1% (Predicted by GENOA 3DP TMg)
D (µm)	20

e) ***Assumption:*** *Damage and Fracture Criteria used for Printed ULTEM 9085 characterization*

Failure Criteria	Damage	Failure
Longitudinal Tensile	Yes	Yes
Longitudinal Compressive	Yes	Yes
Transverse tensile	Yes	Yes
Transvers Compressive	Yes	Yes
Normal Compressive	Yes	Yes
In-Plane Shear	Yes	Yes
Normal Tensile	Yes	Yes
Transverse Normal Shear	Yes	Yes
Longitudinal Normal Shear	Yes	Yes

f) ***Output:*** *Printed ULTEM 9085 material mechanical properties prediction by multi-scale material/structural Nano-mechanics*

Property	Predicted Material Properties by MCQ (MPa)
S11T: Longitudinal Tensile Strength	118.46
S11C: Longitudinal Compressive Strength	152.77
S22T: Transverse Tensile Strength	118.46
S22C: Transverse Compressive Strength	152.77
S33T: Out-of-Plane Tensile Strength	118.46
S33C: Out-of-Plane Compressive Strength	151.25
S12S: In-Plane-Shear	104.24
S13S, S23S	103.21
E11, E22, E33: Longitudinal, Transverse & Out-of-Plane Modulus	2647
G12, G13, G23	947

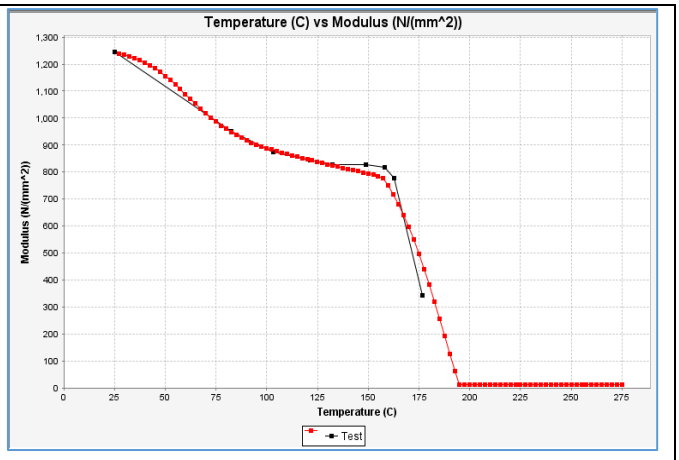
Figure 10. Material Modeling: input to Nano-Assisted Micro-Mechanics analysis

3.2.2 Modulus Property Prediction at Elevated Temperature

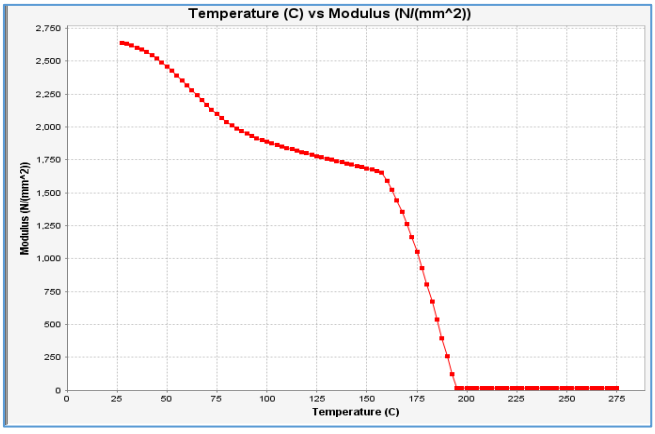
Next, temperature dependent material properties are calculated using cure kinetics approach and compared with test provided in the literature [11]. The data was for a test on a printed FDM ULTEM 9085 cylinder. **Assumption:** The cure kinetics are dependable from the geometry and void content and the same parameters could be used for different geometries with the same material. Considering this assumption, the cure kinetics first was predicted and validated for an arbitrary geometry (FDM printed cylinder with micro and macro voids) and then applied for the baseline material properties (ULTEM 9085 including 1 % micro void content) to predict the modulus for elevated temperatures. **Assumption**: The cure parameters are calibrated to output temperature dependent modulus to show similar behavior as test. **Output:** Temperature dependent resin Modulus property even beyond glass transition temperature of ULTEM 9085 (~186 ºC).

Inputs: *FDM Cylinder Printed ULTEM 9085 validated cure kinetics*

Parameter	Value
Uncured Elastic Modulus	1.244 GPa
Complete Point of Resin Cure	0.8
Resin Chemical Shrinkage in Specific Volume of The Resin occurring Until Diffusion	1
A1-Pre exponential factor	3.5016 E7 Sec^{-1}
A2-Pre exponential factor	-2.5 E7 Sec^{-1}
A3-Pre exponential factor	3.6 E7 Sec^{-1}
DE1-Activation Energy	67 mJ/MOL
DE2-Activation Energy	61.5 mJ/MOL
DE3-Activation Energy	92 mJ/MOL
Time Determined with Degree of Cure	0.35
Total Volume Shrinkage in Curing 1-3 for Epoxy (percent)	2 %
Curve Fitting Constant	7.9 E-20 MPa* Sec^{-1}
Activation Energy for Viscosity	90.8 mJ/MOL
Viscosity Constant (independent of temperature)	141



*Prediction/Test **[11]**: Modulus Vs. Temp No Void*



Prediction/Test: Modulus Vs. Temp with 1% Void (Porous)

Figure 11. Predicted Modulus of ULTEM 9085 at ET

3.2.3 Multi-Factor Plot of Strength

The multi-factor coefficients were varied for each temperature case ($\alpha_{49.9C}$ = 0.4, $\alpha_{59.91C}$ = 0.48, $\alpha_{77.41C}$ = 0.59, $\alpha_{99.92C}$ = 0.52 and $\alpha_{157.4C}$ = 0.269, α_{180C} = 0.3605). For each temperature case progressive failure was performed for both longitudinal and transverse tensile and compressive as well as shear condition and final strengths were estimated. The predicted strength properties are shown in **Figure 12.**

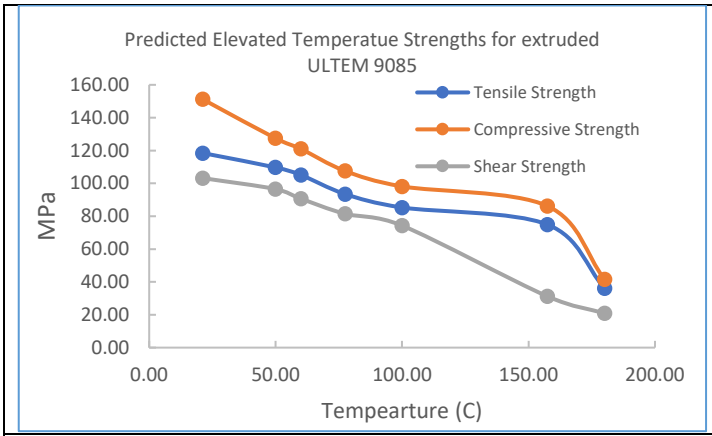
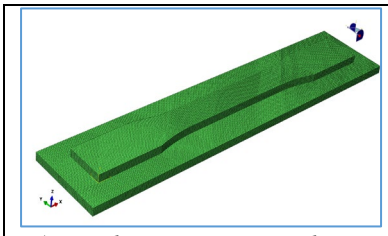


Figure 12. Elevated temperature strengths prediction of FDM extruded ULTEM 90845

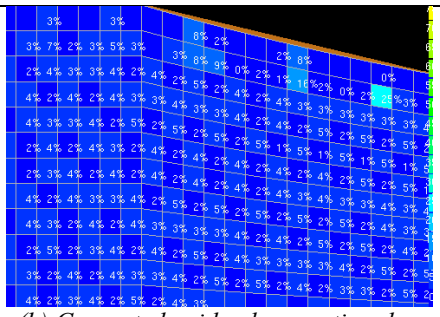
The properties cannot be calculated beyond glass transition temperature based on multi-factor technique. The tensile and compressive strength properties are assumed for higher temperatures equal to ones in Tg. A UMAT card was generated based on temperature dependent ULTEM 9085 mechanical properties. The UMAT card was implemented in the FE model to perform coupled thermal and structural thermal analysis.

3.3 GENOA 3DP PATHCOVERAGE The result of accounting for the reduction of mechanical properties due to these macro voids is shown in the same figure. **Figure 13a**, GENOA 3DP PathCoverage predictions are corroborated by the presences of macro-voids in the printed part. **Figure 13b** provides a close-up of the predicted gaps and the size of each gap as a percentage area of that element. The remaining images provide validation for the accuracy of the software.

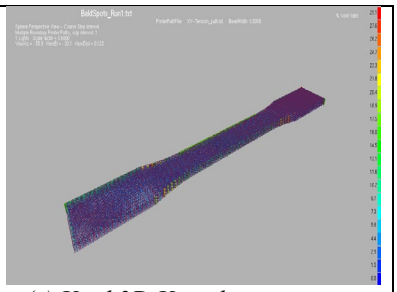
This tool was also implemented to predict bald spots and degrade both the modulus and strength accordingly in element level. Finally, the process was followed by service loading to qualify the part and to predict the part performance.



a) Dog-bone specimen and Base Plate FE Mesh



(b) Computed void volume ration due to anomalies and bald spots for all 6 layers



(c) Void 3D Visualization using GENOA 3DP TMg

Figure 13. FE Model generation, Macro Void Calculation and Visualization

3.4 FDM Printing Process Modeling

The process modeling includes generation of thermal analysis model and sequentially coupled structural thermal analysis model. GENOA 3DP PathCoverage tool was also used to implement the predicted bald spots and degrade both the modulus and strength according to the G-code. Both the analyses were performed to calculate the temperature distribution as well as deformation and

residual stress during the printing process. Summary of the inputs for process modeling is shown in table.

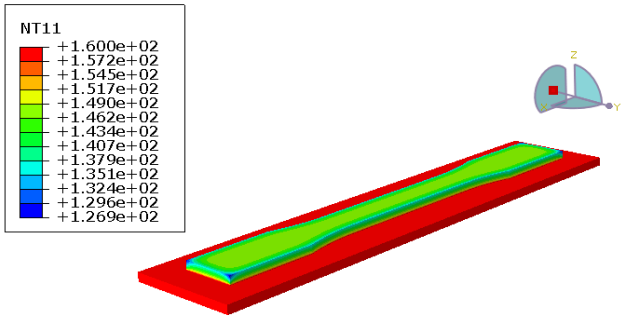
Input: Summary of Slic3r settings	
Property	**Magnitude**
Slic3r Setting	**Adjustment**
Layer height & First layer height	0.536mm
Fill density	100%
Infill pattern	Rectilinear
Fill angle	-/+ 45°
Nozzle diameter	0.65mm
G-code Flavor	Rep-rap
Infill Print Speed	60 mm/s
Perimeter Print Speed	60 mm/s
Nozzle Diameter	0.65 mm

Assumptions: Print Parameters	
Property	**Magnitude**
Bead Width	0.6 mm
Nozzle Temperature	350 °C
Reference Temperature	186 °C
Chamber Temperature	100 °C
Printed Part Convection Coefficient	30 W/(m^{2}K)
Emissivity Coefficient	0.9
Bottom Plate Temperature	160 °C
Bottom Plate Thickness	3.251 mm
Bottom Plate Convection Coefficient	12.5 W/(m^{2}K)
Bottom Plate Emissivity Coefficient	0.45

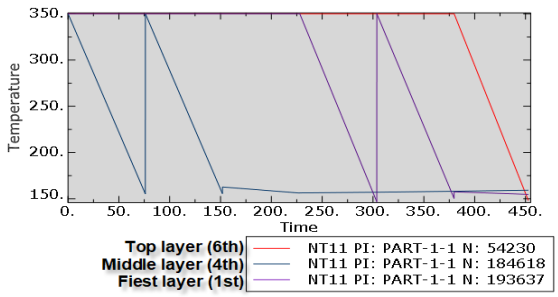
Figure 14. Inputs to generate G-code and Finite Element Model for FDM print process modeling

3.4.1 Thermal Analysis

A commercially available tools was used to generate an input file for thermal and structural-thermal analyses composed of meshed model based on the imported G-code and user defined Temperature dependent material card. An FE solver was then used to execute thermal analysis and determine the temperature distribution on the printed part during FDM printing process. The output from thermal analysis was used as an input to the coupled thermal-structural analysis. The temperature contour fields for build direction (XY) at the end of last printed layer (layer #6)_ is shown in **Figure 15a**. Also, the thermal history of the locations on 1st, 4th and last layers are shown in **Figure 15b**.



a) Temperature contour at end of print process (XY dir)

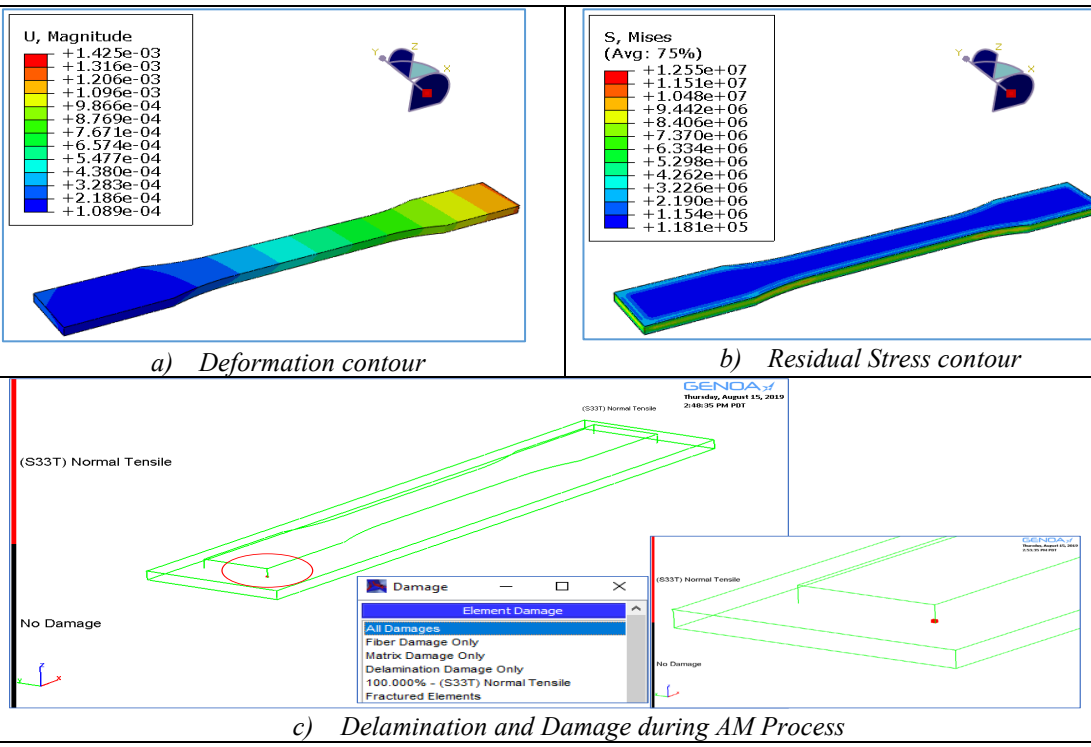


b) Plot of Thermal History through the thickness at center of specimen

Figure 15. Thermal Profile (FEM) and History for build direction XY

3.4.2 Coupled Thermal-Structural Analysis – Residual Stress & Deformation

The uncoupled thermal analysis results were used in a sequentially coupled thermal-structural analysis to predict possible residual stress, deformation, and damage/delamination. The deformation results for different build directions are illustrated in **Figure 16a**. The residual stress of the specimen is shown in **Figure 16b**. Damages on the printed part derived from delamination is also predicted and shown in **Figure 16c.** The predicted residual stresses and deformations from coupled structural-thermal analysis are carried over to service load analysis to provide useful information about the performance of the structure under service loading.



a) Deformation contour *b) Residual Stress contour*

c) Delamination and Damage during AM Process

Figure 16. Process Model: Coupled Thermal-Structural Analysis – Residual Stress, Deformation, and Damage

3.5 Service Load – Damage/Delamination

3.5.1 Dog Bone Specimen

In service loading step, tensile load was implemented to 3D printed part to calculate the load-displacement curve and deformation and was validated with available test results. Additionally, damage initiation and evolution were also calculated. **Figure 17** Shows the gage length, distance between grips (ASTM D638), fixed and load nodes selections representing the edges held by the grips. Tensile test simulation was performed at room temperature for flat (XY) build direction. The FE model description, assumptions are also shown in **Figure 17**. **Figure 18** shows Dog bone deformation and stress contours, load displacement curve, validation of stress-strain curves with the tests at Room Temperature Dry (RTD) from **[8]** and **[9]**. Also, the fracture location and the damage index and plot are shown once the fracture occurs in the simulation (**Figure 18**).

Assumption: *Damage and Fracture Criteria used for Printed ULTEM 9085 characterization*

Failure Criteria	*Damage*	*Failure*
Longitudinal Tensile	*Yes*	*Yes*
Longitudinal Compressive	*Yes*	*Yes*
Transverse tensile	*Yes*	*Yes*
Transvers Compressive	*Yes*	*Yes*
Normal Compressive	*Yes*	*Yes*
In-Plane Shear	*Yes*	*Yes*
Normal Tensile	*Yes*	*Yes*
Transverse Normal Shear	*Yes*	*Yes*
Longitudinal Normal Shear	*Yes*	*Yes*

Input: *FE model for ASTM D638*

Number of Nodes	*233742*
Number of Elements	*55800*
Element type	*C3D8R*

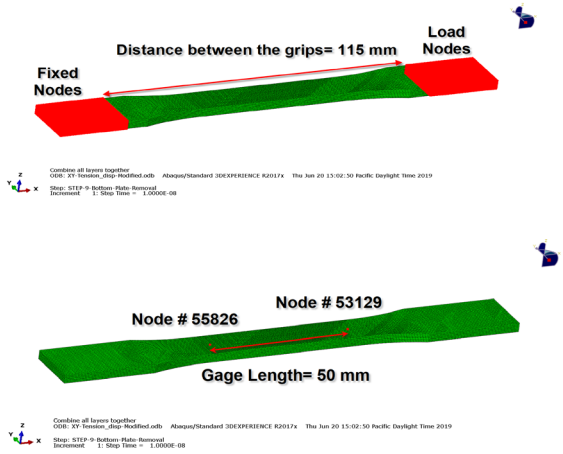
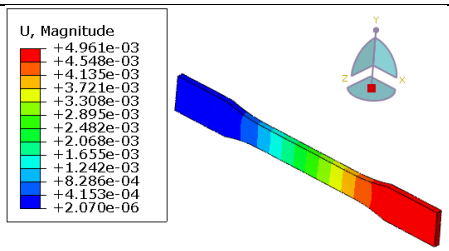
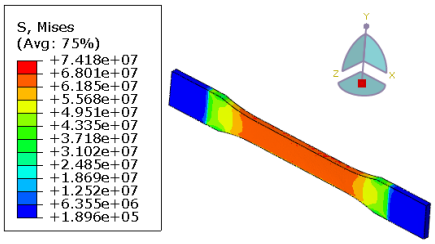


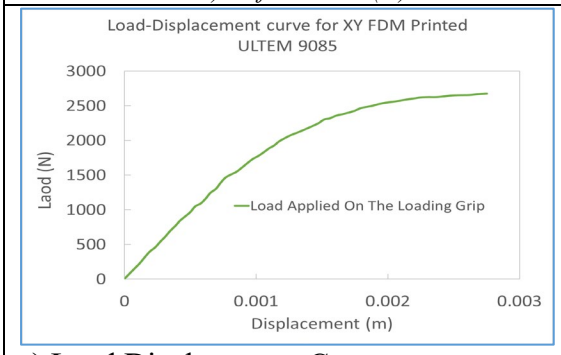
Figure 17. Illustration of FE models specifications, gage length, distance between grips (ASTM 6038). Fixed and load nodes selections and assumptions: Failure criteria



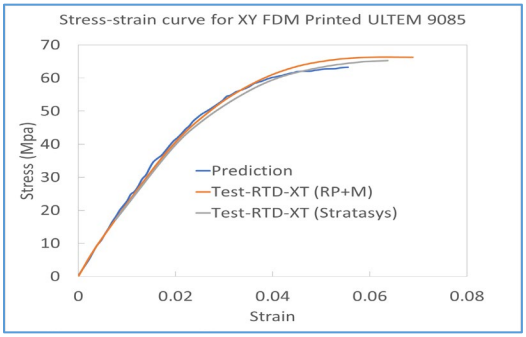
a) Deformation (m)



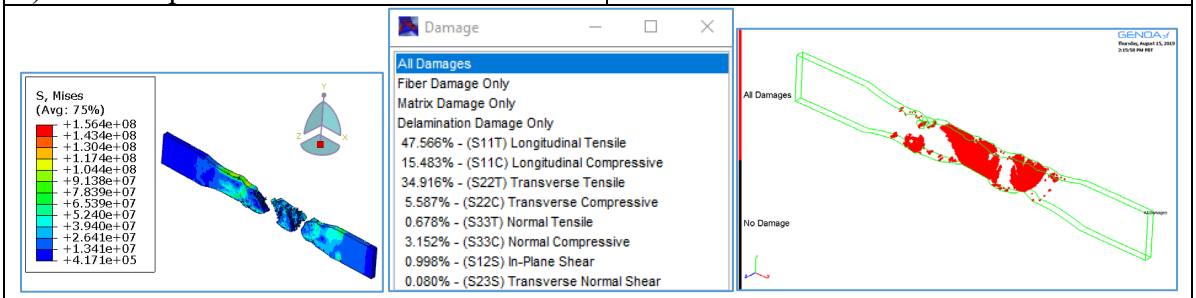
b) Dog Bone stress contour before failure



c) Load Displacement Curve



d) Stress-Strain Comparison with test



e) Fracture locations, damge index and plots

Figure 18. Outputs: Service Loading results

3.5.2 Cross Box Beam Subcomponent

A cross box beam (design courtesy of Made In Space, Inc.) was simulated using the same material system. The inputs and assumptions for the 3D printing simulation as well as the key results (residual stress and part deformation) are shown in **Figure 19**.

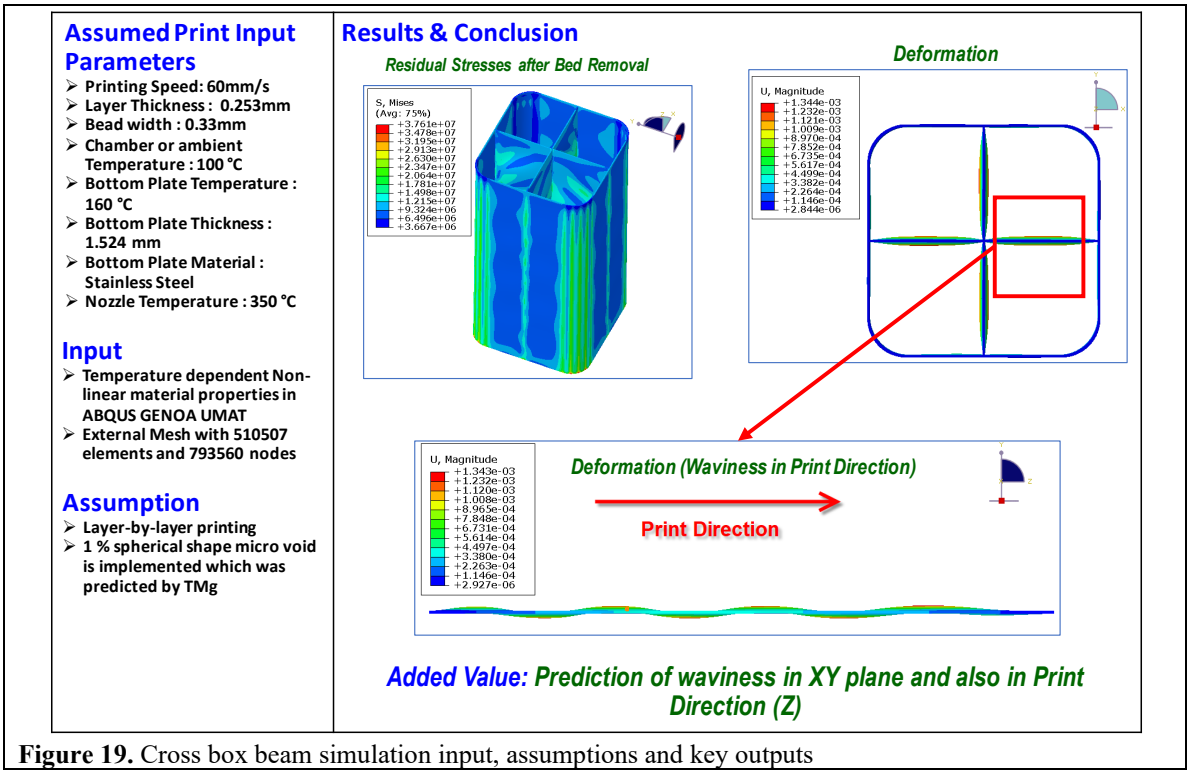


Figure 19. Cross box beam simulation input, assumptions and key outputs

This deformation profile was exhibited in one of the test articles printed by Northrop Grumman Corporation, see **Figure 20**. The deformed wavy pattern shape shown in **Figure 19** shows a very good comparison to actual printed part (**Figure 20**) from quantitative point of view. Further investigation into this behavior and predictive capability is necessary to make any conclusions of accuracy.

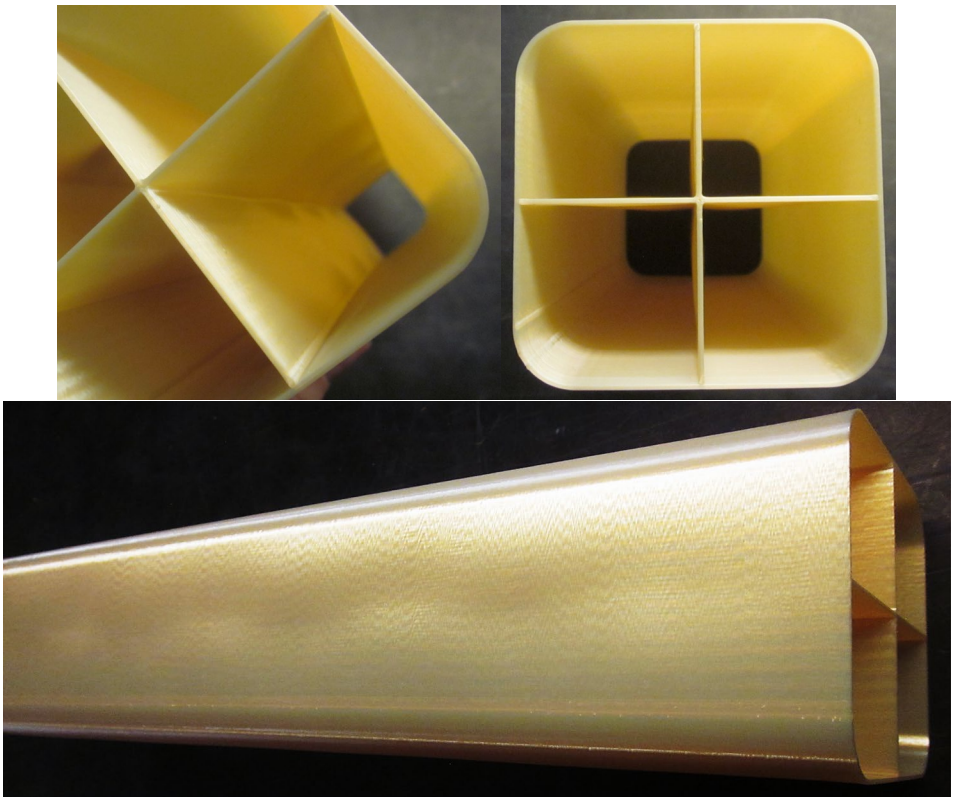


Figure 20. Cross box beam test article with deformation profile printed at Northrop Grumman Corporation

3.6 Material Allowable Generation, and Generic Basis Equivalency

Figure 21 compare the predicted stress-strain of AM printed specimen at XY, XZ, ZX, and ZX45 at RT using Multiscale Progressive Failure Analysis with test curves (Black=Test, Red=Simulation). The inputs are the extruded ULTEM 9085 properties (**Figure 10f**) and the assumptions which is showed in **Table 2** are applied.

Table 3 and Table 4 show the coefficient of variation and distribution type for the mechanical properties of extruded ULTEM 9085 as well as the overall void in the structure of printed specimens by **RP+M** and **Stratasys** Machines respectively.

Table 2. Assumptions: Calibration of material and void properties to predict the effect of print orientation on the Stress-Strain curve of Printed ULTEM 9085

Print Orientation	Pressure constant	EPS11T (Longitudinal tensile strain limit)	Average void volume ratio
XY	0	0.0623	0.056
XZ	-0.45	0.055	0.02
ZX	0.25	0.04	0.03
ZX45	0.15	0.0303	0.03

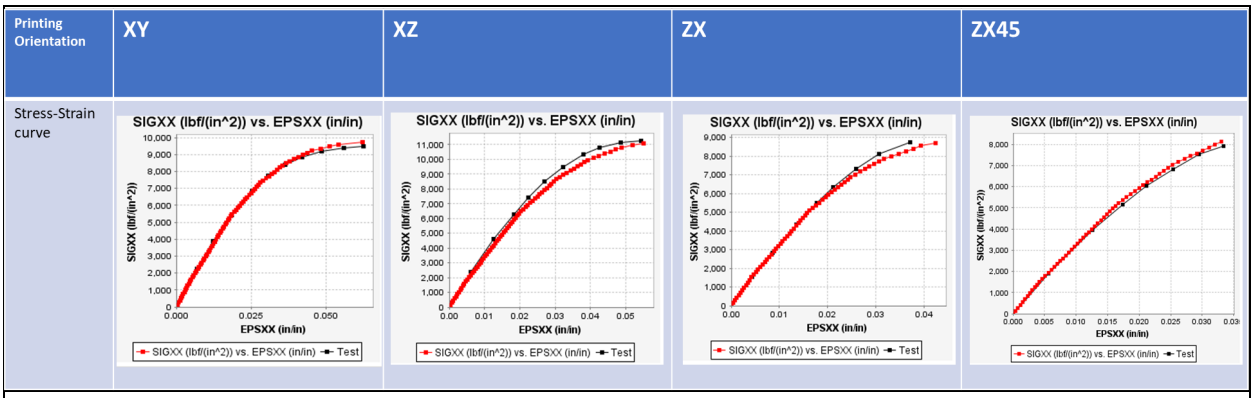


Figure 21. Calibration and validation of Stress-Strain curves of Multiple FDM Print orientation of ULTEM 9085

Table 3. XY Printed Ultem9085 RP+M machine: Coefficient of variables of constituents

Property	Mean Value	Coefficient of Variation (Factor)	Standard Deviation	Distribution type
Tensile Strength (lbf /in^2)	1.718204E+04	0.05	8.591020E+02	Normal
Compressive Strength (lbf /in^2)	2.193826E+04	0.05	1.096913E+03	Normal
Shear Strength (lbf /in^2)	1.496978E+04	0.05	7.484890E+02	Normal
Poisson's ratio	3.975040E-01	0.05	1.987520E-02	Normal
Elastic Modulus ((lbf /in^2)	3.839236E+05	0.05	1.919618E+04	Normal
EPS11T (Longitudinal tensile strain limit)	6.239009E-02	0.28	1.746923E-02	Normal
Void Volume Ratio	0.056000	0.05	0.002800	Log Normal

Table 4. XY Printed Ultem9085 Stratasys machine: Coefficient of variables of constituents

Property	Mean Value	Coefficient of Variation (Factor)	Standard Deviation	Distribution type
Tensile Strength (lbf /in^2)	1.718204E+04	0.05	8.591020E+02	Normal
Compressive Strength (lbf /in^2)	2.193826E+04	0.05	1.096913E+03	Normal
Shear Strength (lbf /in^2)	1.496978E+04	0.05	7.484890E+02	Normal
Poisson's ratio	3.975040E-01	0.05	1.987520E-02	Normal
Elastic Modulus ((lbf /in^2)	3.839236E+05	0.05	1.919618E+04	Normal
EPS11T (Longitudinal tensile strain limit)	6.239009E-02	0.35	1.746923E-02	Normal
Void Volume Ratio	0.056000	0.15	0.008400	Log Normal

Table 5 shows the Cumulative Distribution Function (CDF) for XY printing direction using *RP+M* and *Stratasys* FDM machines. The sensitivity of mechanical properties of Extruded ULTEM 9085 and the overall void content role to determine the ultimate strength of the specimens for each machine is also showed in Table 5.

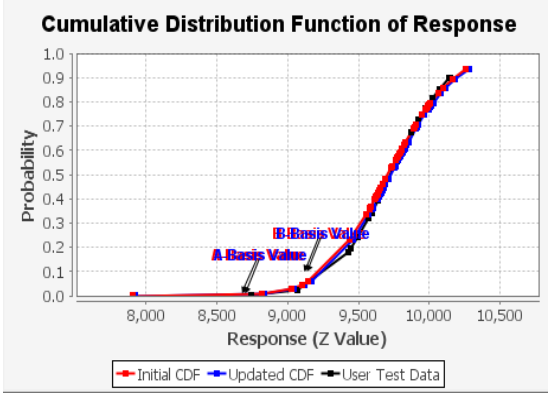
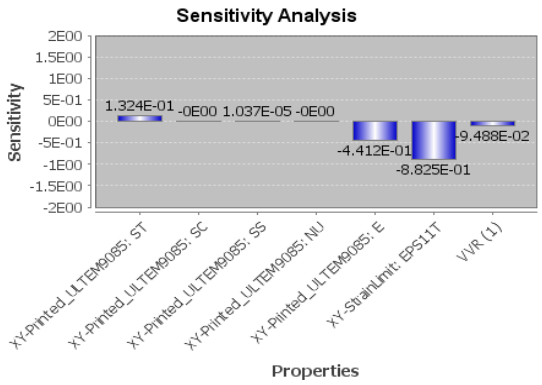
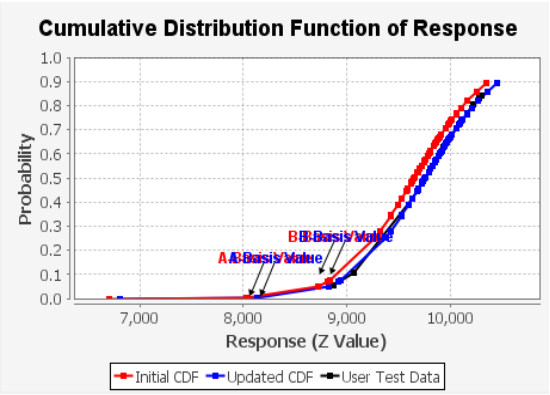
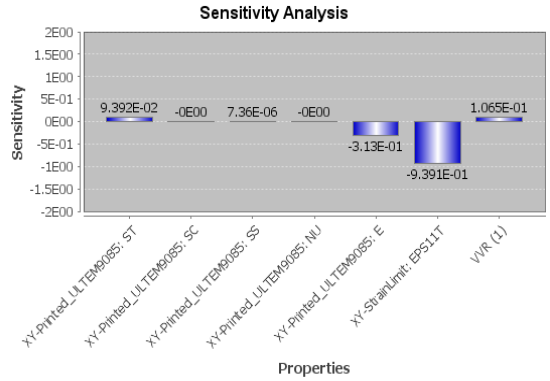
Table 5. *Results of CDF and Sensitivities in all printing orientations*		
Machine	**Cumulative Distributution Function (CFD)**	**Sensistivity Results**
RP+M		
Stratasys		

Table 6 shows the comparison of virtual samples generation method and using test samples to determine the Printed ULTEM 9085 allowables in different printing orientation. **Table 6** shows that there is a good agreement between the allowables predicted and those measured in NIAR test report. The CFD of the generated samples was also updated using Bayesian method to comply with the test samples trend, however, did not change the magnitudes drastically and the initial predictions were in good range. Any outlier sample must be investigated regarding cause and effect on application before deciding what to do or rejected as not being equivalent.

The generated virtual sample parts strengths printed by *Stratasys* and *RP+M* were used to plot the generic acceptance region. This region indicated inside the ellipses defined by blue dots is the generic acceptance region (**Figure 22**).

Table 6. test prediction and validation of A- and B-basis allowables in tension for two different Machines (RP+M, and Stratasys) * Different methods to define allowables in test and simulation

Printing Orientation case	RP+M Fabrication Facility (Psi)										Stratasys Fabrication Facility (Psi)			
	A-Allowable					B-Allowable					A-Allowable		B-Allowable	
	Prediction by MCQ (Normal)		Estimation in NIAR report	test results Analytical method	Error %	Prediction by MCQ (Normal)		Measured in NIAR report	test results Analytical method	Error %	Prediction by MCQ (Normal)		Prediction by MCQ (Normal)	
	Initial	Updated by **Bayesian method**	Basis values and estimates			Initial	Updated by **Bayesian method**	Basis values and estimates			Initial	Updated by **Bayesian method**	Initial	Updated by **Bayesian method**
XY	8917.181	8928.883	8205	ANOVA	8.82*	9257.459	9269.162	8827	ANOVA	5*	8059.2673	8164.115	8737.368	8842.217
XZ	9952.455	10011.574	9145	ANOVA	9.47*	10452.119	10511.238	9977	ANOVA	5.35*	9950.087	10215.312	10450.927	10716.152
ZX	8070.224	8052.497	7972	Normal	1	8283.923	8266.196	8214	Normal	0.63	6849.338	6883.071	7533.272	7567.006
ZX45	6987.190	6769.837	6009	ANOVA	12.66*	7492.988	7275.635	6802	ANOVA	6.96*	6850.399	7187.431	7388.452	7725.484

4. CONCLUSIONS

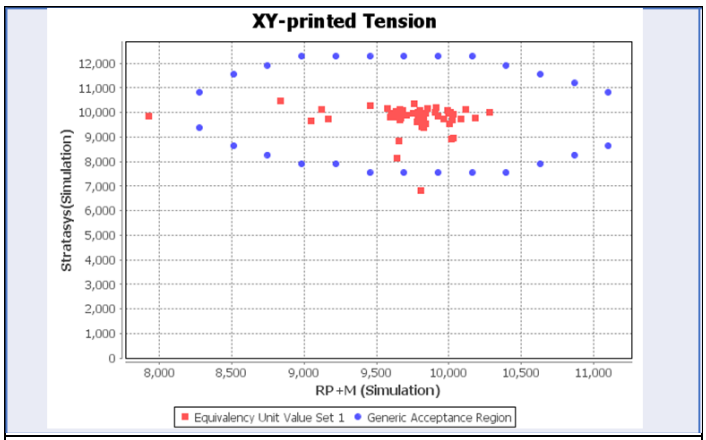


Figure 22. Generic basis Allowables and acceptance region for FDM printed ULTEM 9085 resulted from MCQ (with virtual sampling) for RP+M and Stratasys manufacturing facilities

An entire 3D printing process of ULTEM 9085 material was presented in this paper. The elevated temperature modulus of Printed ULTEM 9085 was predicted and validated and temperature dependent material properties were calculated using predicted coupled cure kinetics and multi factor technique. The calculated properties were implemented in 3D printing process modeling (coupled structural-thermal analysis) to calculate residual stresses and deformation. This method would let the manufacturers to predict the possible deformation in the printed parts and adjust the machine parameters to compensate or minimize it. Further, tensile service loading was applied on the simulated printed dog-bone in XY orientation and the results of stress curve was validated. The whole method could be used to simulate printing of parts with different geometries and apply service loading to evaluate the design virtually which contributes to cost reduction. The strength allowables of printed ULTEM 9085 using RP+M and Stratasys were predicted and the results were validated with tests. Also, the generic acceptance region lets the designers know the probable strength region of two (or multiple) printed machines or manufacturing facilities so they can design the parts and components accordingly considering the effect of machines on the quality of printed parts.

5. REFERENCES

1. Zaldivar, R. J., D. B. Witkin, T. McLouth, D. N. Patel, K. Schmitt, and J. P. Nokes. "Influence of processing and orientation print effects on the mechanical and thermal behavior of 3D-Printed ULTEM® 9085 Material." Additive Manufacturing 13 (2017): 71-80.
2. Lužanin, Ognjan, Dejan Movrin, and Miroslav Plančak. "Effect of layer thickness, deposition angle, and infill on maximum flexural force in FDM-built specimens." Journal for Technology of Plasticity 39, no. 1 (2014): 49-58.
3. Taylor, G., Wang, X., Mason, L., Leu, M.C., and Chandrashekhara, K., "Investigation of Ultem 1010 FDM sparse-build parts using design of experiments and numerical simulation," in Proceedings of The Composites and Advanced Materials Expo, Anaheim, CA, September 26-29, 2016.
4. Ji, L.B., and Zhou, T.R., "Finite element simulation of temperature field in fused deposition modeling." Advanced Materials Research, Vol. 97, pp. 2585-2588, 2010.
5. Górski, F., Kuczko, W., Wichniarek, R., and Hamrol, A., "Computation of mechanical properties of parts manufactured by Fused Deposition Modeling using finite element method." In 10th International Conference on Soft Computing Models in Industrial and Environmental Applications, Springer International Publishing, pp. 403-413, 2015.
6. Taylor, G., Wang, X., Mason, L., Leu, M.C., and Chandrashekhara, K., "Optimization of ULTEM 1010 fused deposition modeling specimens for flexural behavior," in Proceedings of The Composites and Advanced Materials Expo, Orlando, FL, December 11-14, 2017.
7. Mori T, Tanaka K. Average Stress in the Matrix and Average Elastic Energy of Materials with Misfitting Inclusions. Acta Metallurgica 1973; 21, p. 571-574.
8. https://www.wichita.edu/research/NIAR/Documents/NCP-RP-2018-007-Rev-NC-ULTEM-9085-Stat-Analysis-Report-April-16-2019.pdf
9. https://www.wichita.edu/research/NIAR/Documents/CAM-RP-2018-027-NC-Stratasys-Certified-ULTEM-Equivalency-FINAL-MPDR-4.17.2019.pdf
10. Chamis, Christos C., Frank Abdi, Mohit Garg, Levon Minnetyan, Harsh Baid, Dade Huang, Jerry Housner, and Farid Talagani. "Micromechanics-based progressive failure analysis prediction for WWFE-III composite coupon test cases." Journal of Composite Materials 47, no. 20-21 (2013): 2695-2712.
11. Li, H., G. Taylor, V. Bheemreddy, O. Iyibilgin, M. Leu, and K. Chandrashekhara. "Modeling and characterization of fused deposition modeling tooling for vacuum assisted resin transfer molding process." Additive Manufacturing 7 (2015): 64-72.
12. T. A. Bogetti and J. W. Gillespie, "Process-induced stress and deformation in thick-section thermoset composite laminates," Journal of composite materials, vol. 26, pp. 626-660, 1992.
13. Blok, L. G., M. L. Longana, H. Yu, and B. K. S. Woods. "An investigation into 3D printing of fibre reinforced thermoplastic composites." *Additive Manufacturing* 22 (2018): 176-186.
14. Hajiha, R, Godines, C, De Fenza, A, Baid, H, Clarkson, E, Moazami, N, Abdi, F. "Allowable Generation and Generic Basis Value for Multiple Loading and Environmental Conditions". CAMX 2019, Anaheim, CA.
15. http://www.sdplastics.com/ensinger/ultem.pdf
16. El-Gizawy, A. Sherif, Shan Corl, and Brian Graybill. "Process-induced properties of fdm products." In Proceedings of the ICMET, International Conference on Mechanical Engineerings and Technology Congress & Exposition. 2011.